

Supplementary Information for

**Graphene Coupled Flower-Like Oxidized-Polyacrylonitrile
as High-Performance Anode for Sustainable Lithium-Ion
Batteries**

Xiaoyan Han*, Zongying Xiao, Kai Chen, Qi Lai, and Yingkui Yang*

*Key Laboratory of Catalysis and Energy Materials Chemistry of Ministry of Education
& Hubei Key Laboratory of Catalysis and Materials Science, South-Central Minzu
University, Wuhan 430074, China*

E-mails: xyhan@scuec.edu.cn (X. Han), and ykyang@mail.scuec.edu.cn (Y. Yang).

Experimental section

Materials

Graphene oxide (GO) was prepared by a modified Hummers' method as described previously (*Energy Environ. Mater.* 2018, 1, 88). Acrylonitrile (ACN) and azobis(isobutyronitrile)(AIBN) were purchased from Sinopharm Chemical Reagent Co., Ltd. All chemicals were used as received without further purification.

Synthesis of OPAN and OPAN@Gr hybrids

An appropriate amount of GO (5 wt.%, 10 wt.%, 20 wt.%) was ultrasonically dispersed into acetone (25 mL, as the solvent). Both ACN (5 ml, as the monomer) and AIBN (5 mg, as the initiator) were then successively added into the above dispersion under constant stirring. The resultant mixture was held in a sealed glass vial for the consecutive reaction at 70°C for 12 h under an Ar atmosphere. After cooling to room temperature, the product was collected by centrifugation and washing with distilled water and ethanol for several times. Subsequently, the dark grey powder of PAN@GO was obtained after drying at 60°C under vacuum for 12 h followed by annealing at 280°C for 3 h in air, giving a black powder of OPAN@Gr. Finally, three OPAN@Gr hybrids (OPAN@Gr-1, OPAN@Gr-2, and OPAN@Gr-3) with different GO contents were obtained through the identical experimental procedures. In control experiments, pure OPAN was also obtained by the same procedure in the absence of GO. Pure PAN was synthesized under identical synthetic conditions in the absence of GO and without subsequent thermal treatment.

Materials characterization

Scanning electron microscopy (SEM) images were obtained on a Hitachi SU-8010 scanning electron microscope (Japan). Transmission electron microscopy (TEM) images were taken on a TALOS F200X electron microscope. Fourier transform infrared (FT-IR) spectra were recorded on a NEXUS 470 spectrometer (Thermo Nicolet, USA). Raman spectrum was examined by a Thermo Scientific DXR spectrometer (Thermo Scientific, USA) with a 532 nm Ar-ion laser. X-ray diffraction (XRD) tests were characterized by Rigaku/MiniFlex 600 diffraction (Japan) in the range of $2\theta = 5\sim 80^\circ$ using a monochromatic Cu K α radiation with a scan rate of 5° min^{-1} . X-ray

photoelectron spectroscopy (XPS) was conducted on a Thermo Multi Lab 2000 spectrometer. The elemental analysis tests were performed on a VARIO Micro Cube.

Electrochemical measurements

CR2032-type coins were used to evaluate the electrochemical performance. The working electrode was fabricated by mixing 60 wt% active materials (OPAN or OPAN@Gr), 30 wt% Super P as conductive carbon, and 10 wt% PVDF as a binder. 1.0 M LiPF₆ in a mixture of ethylene carbonate and diethyl carbonate (v/v = 1/1) was used as the electrolyte. The copper foil was used as current collector, the Celgard 2500 porous membrane as the separator and the lithium foil was used as the counter electrode. The mass loading of active materials on each electrode ranged from 0.8 to 1.2 mg cm⁻². The discharge/charge tests were performed on a Land CT2001A battery testing system between 1.5 and 3.5 V. The charge/discharge capacities were calculated based on the mass of active materials (OPAN or OPAN@Gr). Cyclic voltammetry (CV) and electrochemical impedance spectroscopy (EIS) were carried out on a CHI 760E electrochemical workstation. CV was performed in the potential range of 1.5 ~ 3.5 V, and EIS was performed in the frequency range of 0.01~105 Hz.

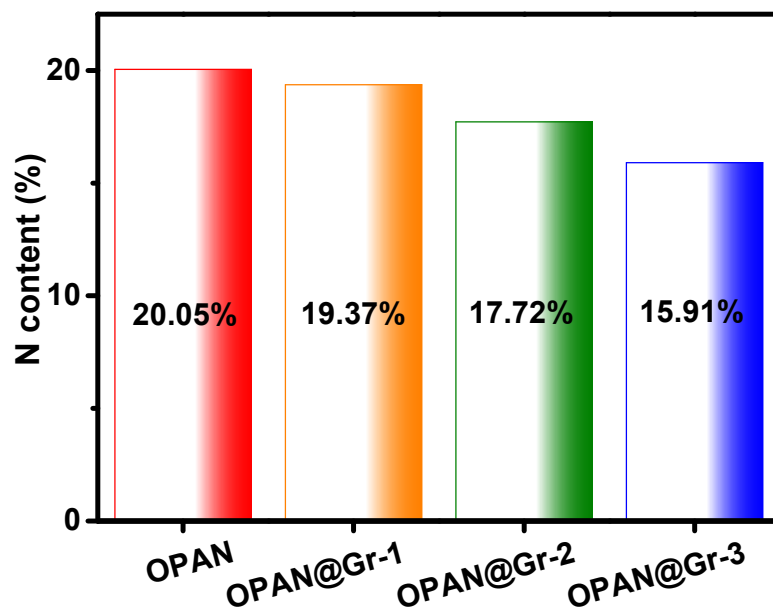


Fig. S1 Elemental N content in OPAN and OPAN@Gr.

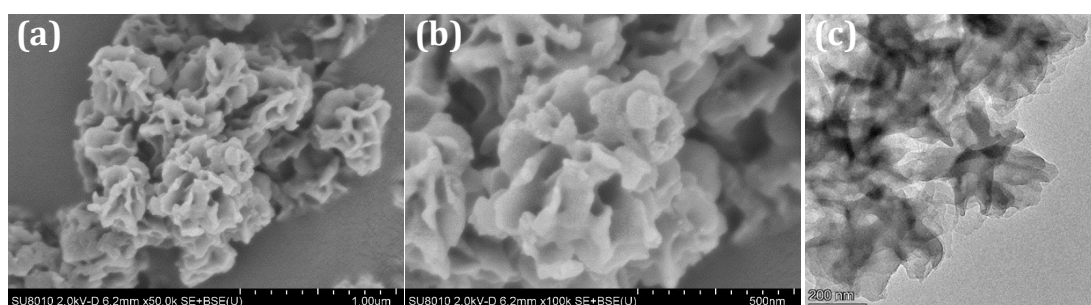


Fig. S2 (a, b) SEM and (c) TEM images of pure OPAN.

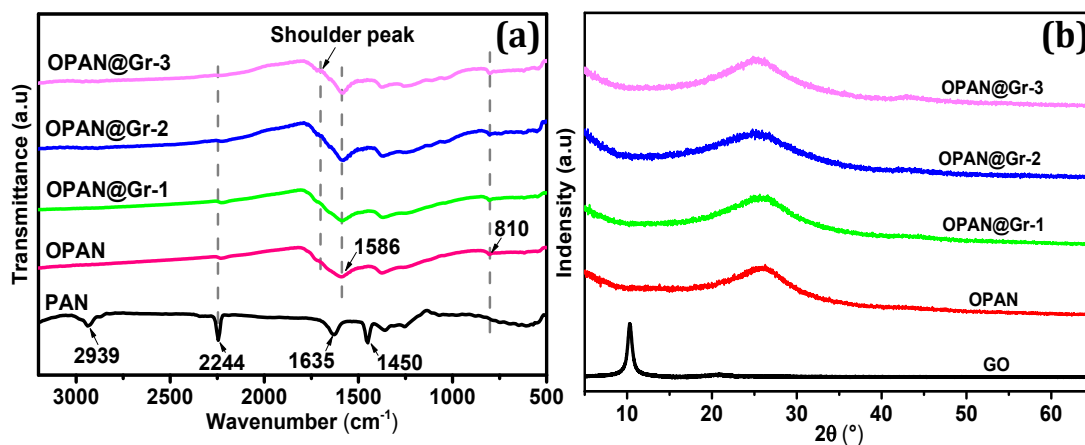


Fig. S3 FT-IR spectra (a) and XRD patterns (b) of PAN, OPAN, GO and OPAN@Gr hybrids.

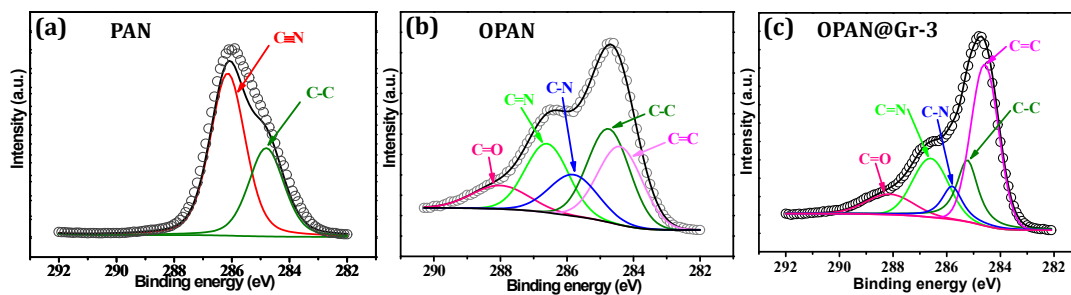


Fig. S4 XPS C1s spectra of PAN (a), OPAN (b) and OPAN@Gr-3 (c).

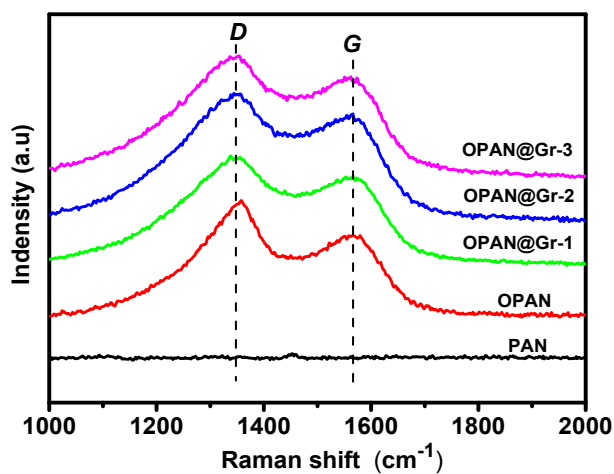


Fig. S5 Raman spectra of PAN, OPAN and OPAN@Gr hybrids.

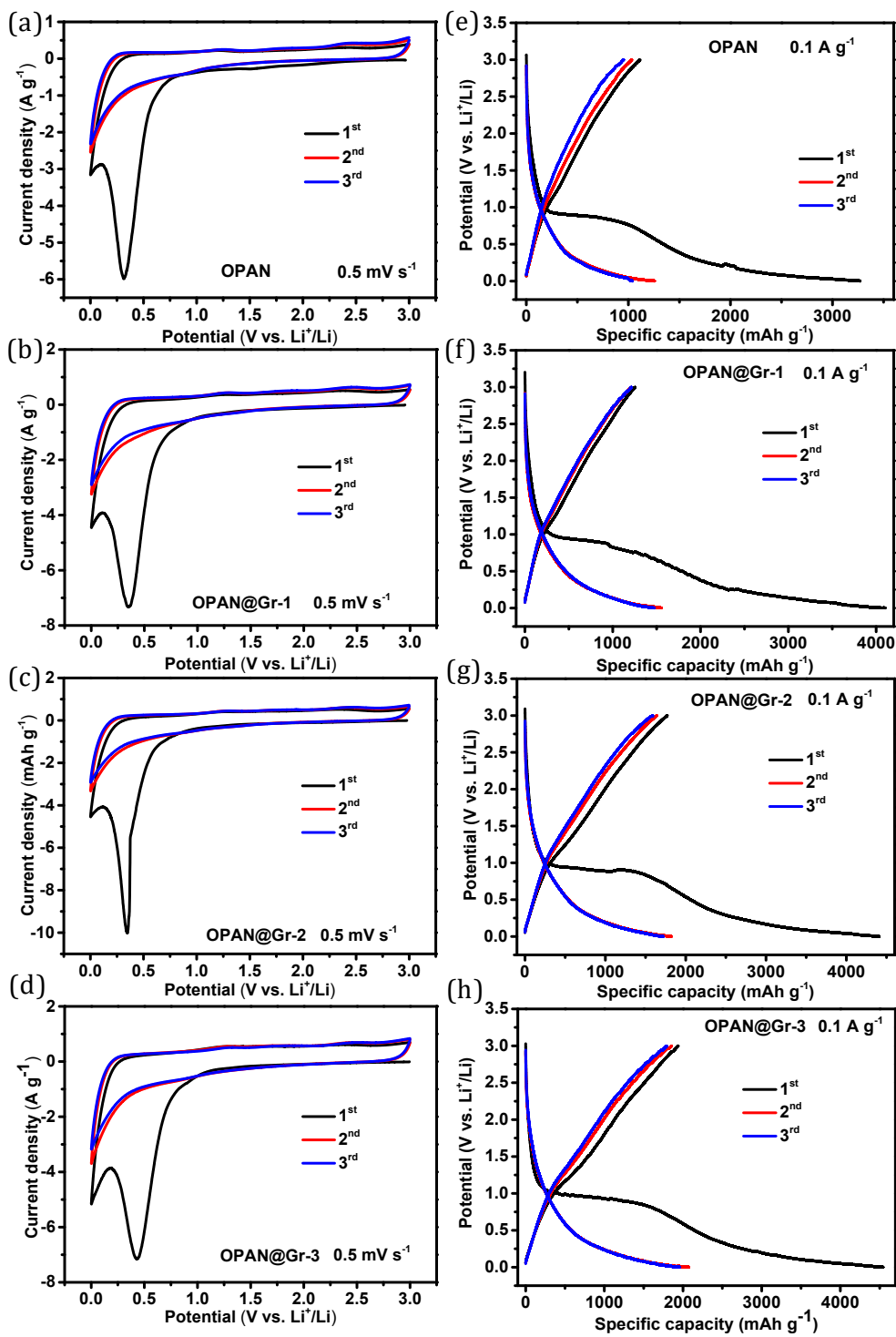


Fig. S6 Typical CV curves and charge/discharge voltage profiles of OPAN and OPAN@Gr hybrids in the first three cycles.

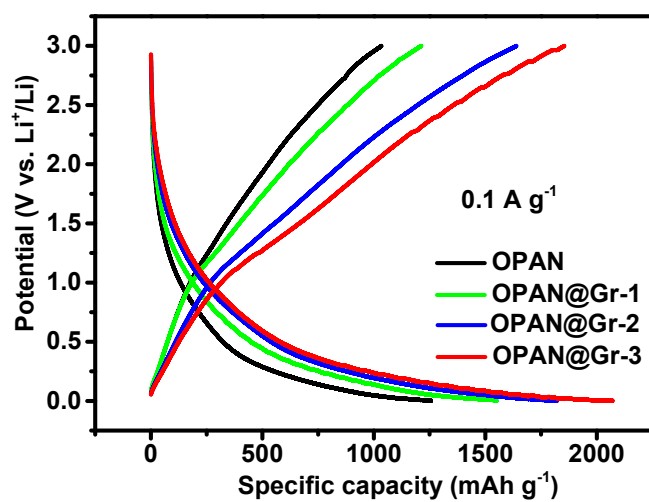


Fig. S7 Charge/discharge voltage profiles of OPAN and OPAN@Gr in the 2nd cycle.

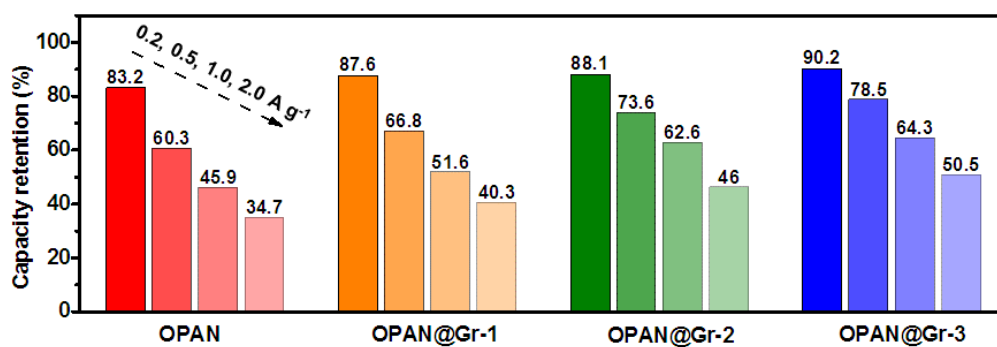


Fig. S8 Capacity retention of OPAN and OPAN@Gr anodes at different current densities.

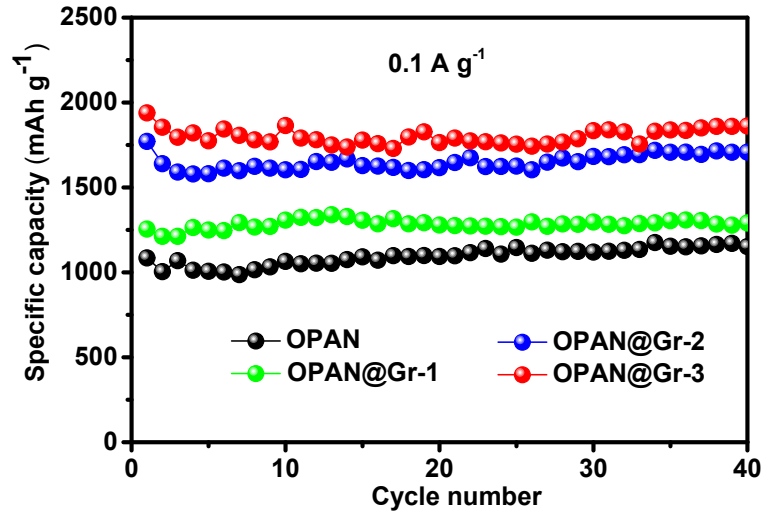


Fig. S9 Cycling stability of pure OPAN and OPAN@Gr hybrids at 0.1 A g⁻¹.

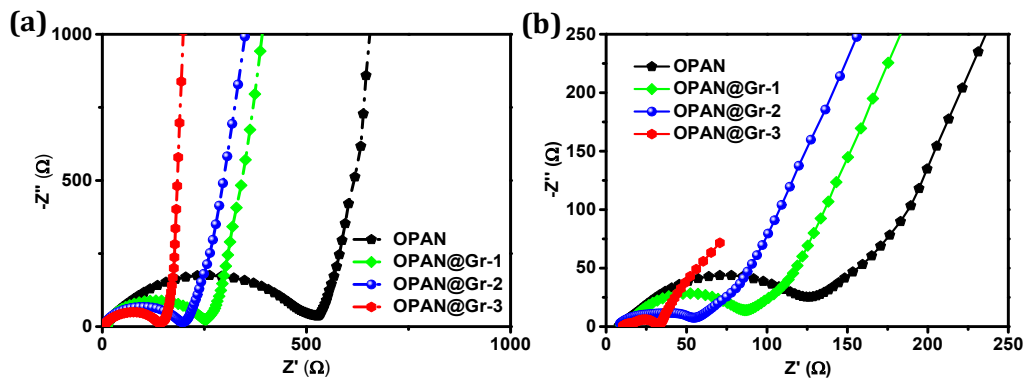


Fig. S10 EIS plots of OPAN and OPAN@Gr hybrids before (a) and after (b) cycles.

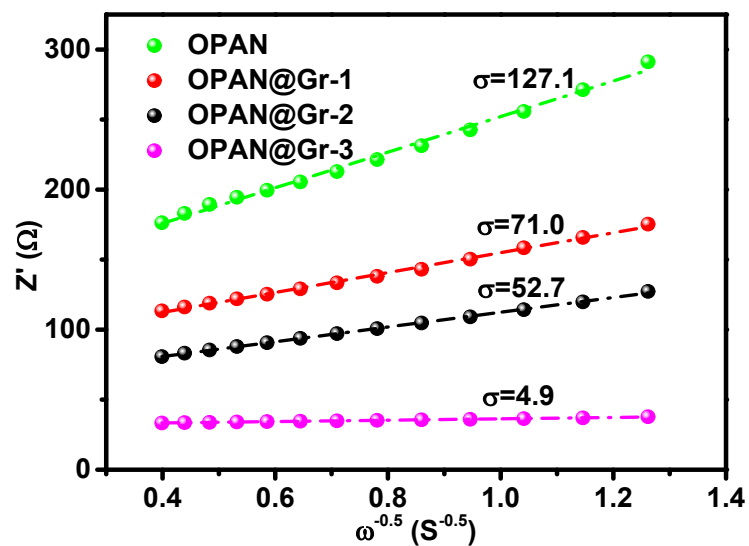


Fig. S11 The linear plots of real parts of complex impedance vs $\omega^{-0.5}$.

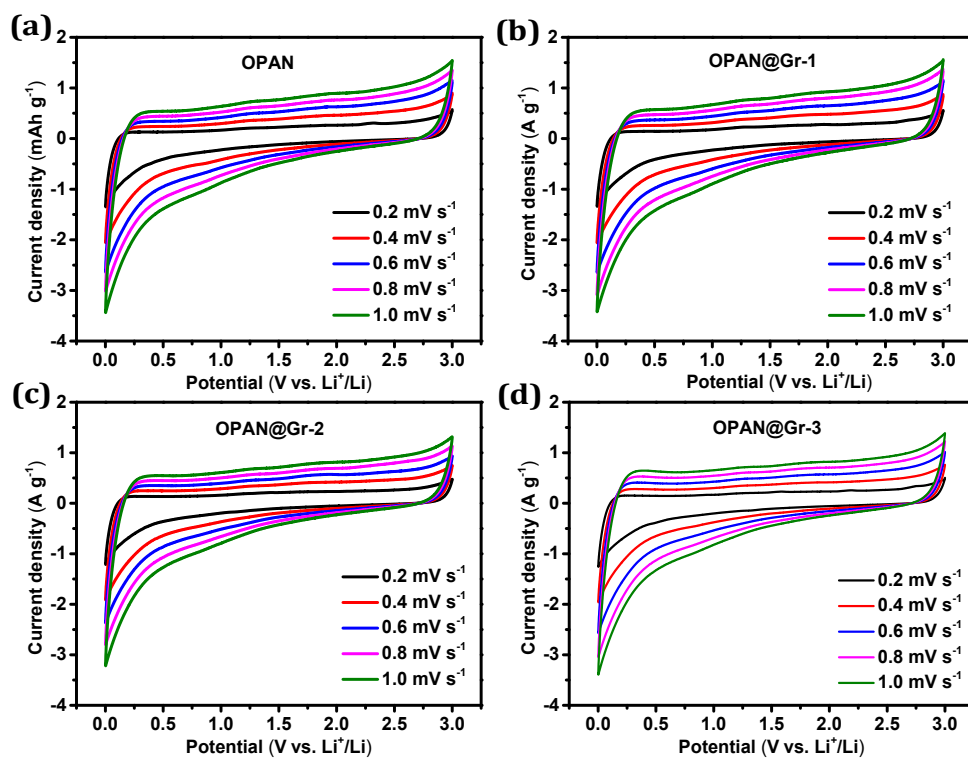


Fig. S12 CV curves of OPAN and OPAN@Gr hybrids at different scan rates.

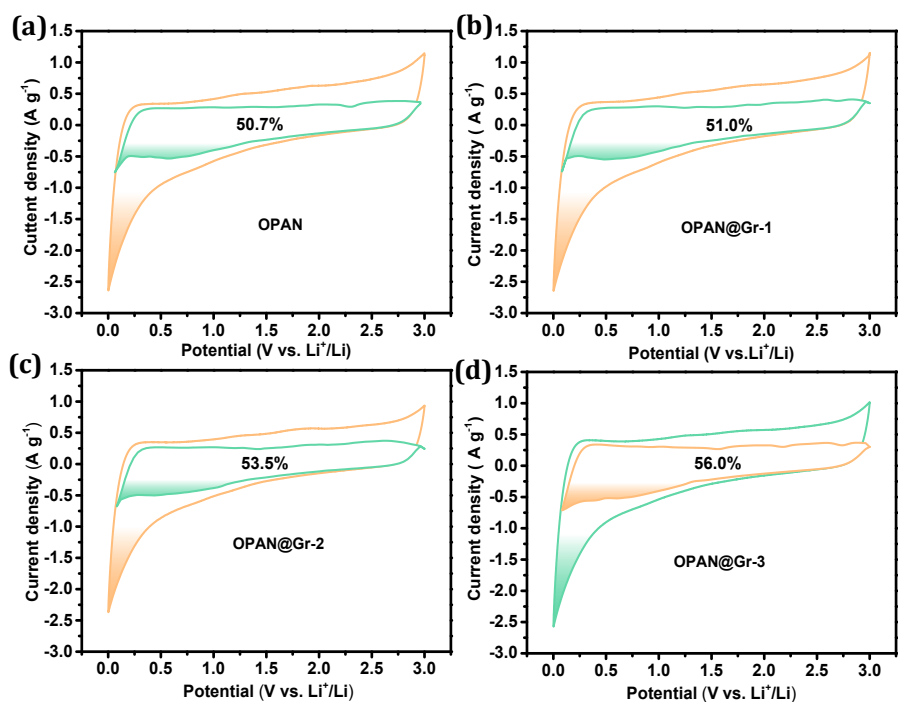


Fig. S13 The decoupling curves of capacitive contribution (shadow) of OPAN and OPAN@Gr anodes at 0.6 mV s^{-1} .

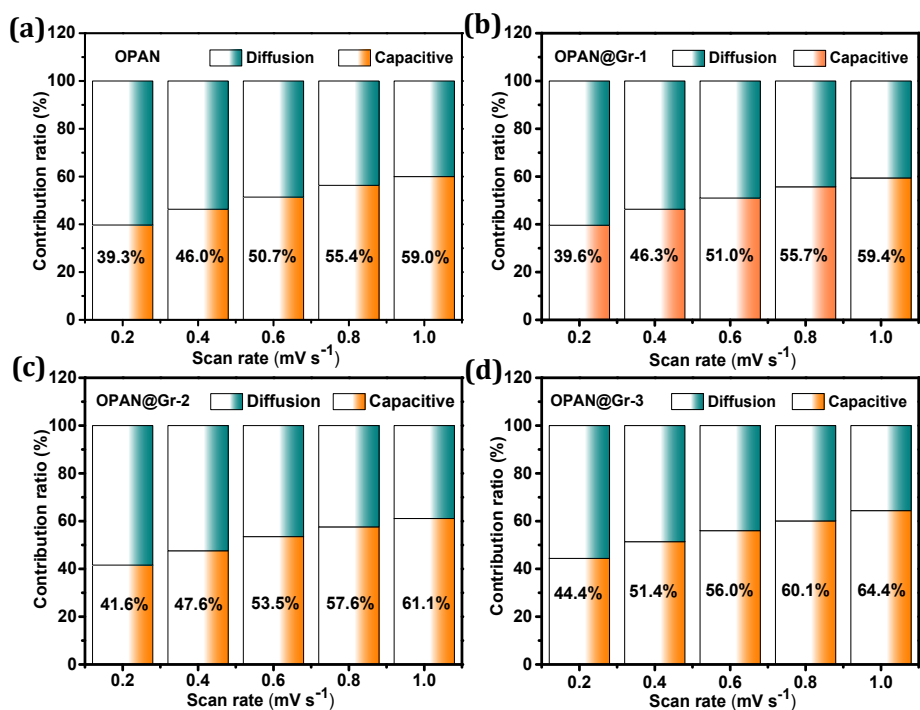


Fig. S14 The capacitive contribution of OPAN and OPAN@Gr at different scan rates.

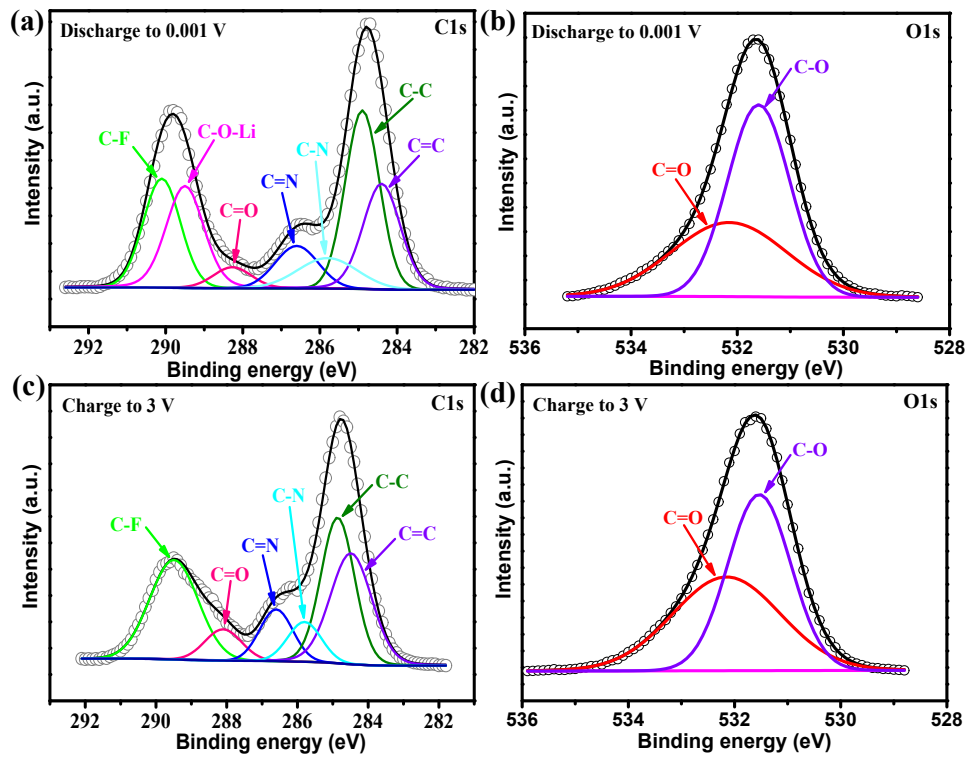
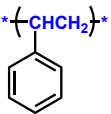
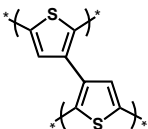
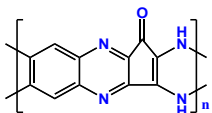
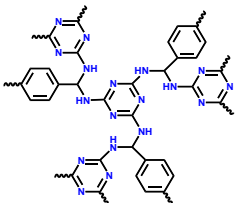
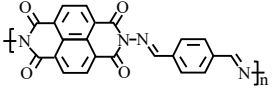
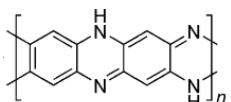
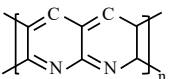
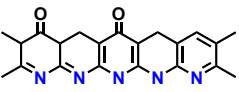


Fig. S15 C1s and O1s XPS spectra of OPAN anodes during the 40th discharge (lithiation) and charge (delithiation) processes.

Table S1 The comparison of typical polymer-based anodes for LIBs

Polymers used	Specific capacity	Rate capability	Cycling stability	Ref.
	149.97 mA h g ⁻¹ /100 mA g ⁻¹	90.38 mA h g ⁻¹ /0.5 A g ⁻¹	67.6% (119.03 mA h g ⁻¹)/100 cycles/0.1 A g ⁻¹	1
	1215 mA h g ⁻¹ /45 mA g ⁻¹	387 mA h g ⁻¹ /5 A g ⁻¹	79.9% (663 mA h g ⁻¹)/1000 cycles/ 0.5 A g ⁻¹	2
	1231 mA h g ⁻¹ /200 mA g ⁻¹	259 mA h g ⁻¹ /2.0 A g ⁻¹	486 mA h g ⁻¹ / 1000 cycles/ 1 A g ⁻¹	3
	1678 mA h g ⁻¹ /100 mA g ⁻¹	419 mA h g ⁻¹ /2.0 A g ⁻¹	87.8% (489 mA h g ⁻¹)/1000 cycles/2.5 A g ⁻¹	4
	132 mA h g ⁻¹ /50 mA g ⁻¹	48 mA h g ⁻¹ /10 A g ⁻¹	203 mA h g ⁻¹ /1000 cycles / 0.5 A g ⁻¹	5
	623 mA h g ⁻¹ /100 mA g ⁻¹	217 mA h g ⁻¹ /2 A g ⁻¹	85.7% (<200 mA h g ⁻¹)/1600 cycles/2 A g ⁻¹	6
	1750 mA h g ⁻¹ /90 mA g ⁻¹	303 mA h g ⁻¹ /9.1 A g ⁻¹	500 mA h g ⁻¹ /1000 cycles /4.6 A g ⁻¹	7
	1176 mA h g ⁻¹ /100 mA g ⁻¹	439 mA h g ⁻¹ /2.0 A g ⁻¹	330 mA h g ⁻¹ /5000 cycles /10 A g ⁻¹	8
	1375 mA h g ⁻¹ /50 mA g ⁻¹	671.3 mA h g ⁻¹ /2 A g ⁻¹	72% (~200 mA h g ⁻¹)/10000 cycles /10 A g ⁻¹	9
	1688 mA h g ⁻¹ /100 mA g ⁻¹	852 mA h g ⁻¹ /2 A g ⁻¹	80% (368 mA h g ⁻¹)/5000 cycles/10 A g ⁻¹	<i>This work</i>

References

- [1] Y. Aldawsari, Y. Mussa, F. Ahmed, M. Arsalan and E. Alsharaeh, *Materials*, 2019, 12, 2248.
- [2] C. Zhang, Y. He, P. Mu, X. Wang, Q. He, Y. Chen, J. Zeng, F. Wang, Y. Xu and J. Jiang, *Adv. Funct. Mater.*, 2018, 28, 1705432.
- [3] Z. Man, P. Li, D. Zhou, R. Zang, S. Wang, P. Li, S. Liu, X. Li, Y. Wu, X. Liang and G. Wang, *J. Mater. Chem. A*, 2019, 7, 2368.
- [4] J. Xie, X. Rui, P. Gu, J. Wu, Z. Xu, Q. Yan and Q. Zhang, *ACS Appl. Mater. Interfaces*, 2016, 8, 16932.
- [5] S. Xu, W. Xu, L. Kong and Y. Zhang, *SN Appl. Sci.*, 2020, 2, 2523-3963.
- [6] J. Wang, H. Yao, C. Du and S. Guan, *J. Power Sources*, 482 (2021) 228931.
- [7] J. Wu, X. Rui, G. Long, W. Chen, Q. Yan and Q. Zhang, *Angew. Chem. Int. Ed.*, 2015, 54, 7354.
- [8] Q. Liu, Z. Xiao, X. Cui, S. Deng, Q. He, Q. Zhang, Z. Lin and Y. Yang, *J. Mater. Chem. A*, 2021, 9, 6962.
- [9] T. Gua, M. Zhou, B. Huang, S. Cao, J. Wang, Y. Tang, K. Wang, S. Cheng and K. Jiang, *Chem. Eng. J.*, 373(2019)501.